PCCP

Cite this: *Phys. Chem. Chem. Phys.*, 2011, **13**, 5053–5060

www.rsc.org/pccp

PAPER

Pore size analysis of >250 000 hypothetical zeolites†

Emmanuel Haldoupis, Sankar Nair and David S. Sholl*

Received 3rd December 2010, Accepted 12th January 2011
DOI: 10.1039/c0cp02766a

Computational methods have been used in the past to generate large libraries of hypothetical zeolite structures, but to date analysis of these structures has typically been limited to relatively simple physical properties such as density. We use efficient methods to analyze the adsorption and diffusion properties of simple adsorbate molecules in a library of >250 000 hypothetical silica zeolites that was generated previously by Deem and co-workers (*J. Phys. Chem. C*, 2009, **113**, 21353). The properties of this library of materials are compared to the complete set of ~190 zeolites that have been identified experimentally. Our calculations provide information on the largest cavities available in each material for adsorption, and the size of the largest molecules that can diffuse through each material. For a subset of ~8000 materials, we computed the Henry's constant and diffusion activation energy for adsorbed CH_4 and H_2. We show that these calculations provide a useful screening tool for considering large collections of nanocrystalline materials and choosing materials with particular promise for more detailed modeling.

Introduction

The ordered nanopores of zeolites and other crystalline nanoporous materials give these materials useful properties for chemical separations and shape-selective catalysis.[1] Small differences in the pore structure can lead to significant differences in the adsorption and transport of molecules in nanopores.[2] It is therefore interesting to understand what range of pore characteristics are possible within well defined classes of nanoporous crystals.

We recently introduced an efficient method that characterizes adsorption and diffusion of simple molecules in nanopores and applied this method to a collection of >500 metal–organic framework materials.[3] Although these calculations give less detailed information than more traditional molecular simulation techniques such as Grand Canonical Monte Carlo and Molecular Dynamics,[4,5] they require far smaller computational resources. This makes our methods appropriate for screening large classes of materials to identify those materials whose properties are sufficiently promising to warrant more detailed studies.

In this paper we used these efficient methods to characterize the pores in >250 000 hypothetical silica zeolites. This large collection of structures was generated recently by Deem and co-workers,[6] and is one example of several efforts to generate libraries of zeolitic materials computationally.[7,8] The structures of Deem *et al.* were found by systematically examining many possible crystal symmetries *via* a force field that defines the energy of each atomic configuration that is considered. The number of structures in this collection exceeds that the number of zeolite structures that have been synthesized experimentally, ~190,[9] by more than a factor of 1000. This difference is even more stark when we note that less than 10% of the experimentally known zeolites have been produced in a pure silica form.

In section 2 we describe our calculation methods and introduce several ways that we have defined subsets of the full collection of silica zeolites that are used in discussing our results. In section 3 we characterize the full collection of >250 000 zeolite structures in geometric terms that define the size of molecules that can adsorb and diffuse in each structure. The range of results found is compared with results for the set of ~190 zeolites that are known experimentally. We have selected ~8000 of the hypothetical materials for more detailed calculations. In section 4, we report the calculated Henry's constants and diffusion activation energy for adsorbed CH_4 in these structures. Our conclusions are summarized in section 5.

Calculation details

The properties of a set of nanoporous materials whose chemical composition is identical are almost entirely controlled by the geometry of each material's pores. Previous efforts to characterize pores in large groups of materials have identified two quantities of special interest.[10] First, the largest cavity diameter (LCD) is the diameter of the largest sphere that can be inserted inside the porous material without overlapping any of the atoms in the material. Molecules with sizes similar to the

School of Chemical & Biomolecular Engineering, Georgia Institute of Technology, Atlanta, GA 30332-0100, USA.
E-mail: david.sholl@chbe.gatech.edu
† Electronic supplementary information (ESI) available. See DOI: 10.1039/c0cp02766a

LCD will typically not be able to diffuse through more constricted regions of the material's pores. This process is controlled by the second quantity, the pore limiting diameter (PLD), which is the diameter of the largest sphere that can diffuse an unbounded distance through the pores without overlapping atoms in the material. In less precise terms, the PLD characterizes the width of the bottlenecks that control what molecules can and cannot diffuse into the pores. If multiple pore channels exist then the pore with the largest pore limiting diameter is called the major pore. The largest cavity in the structure, denoted as the global cavity diameter, is not necessarily equal to the largest cavity diameter along the major pore.

The LCD and PLD are defined by describing adsorbing molecules and atoms in the porous materials as hard spheres, where the concept of overlap is well defined. The interactions of real atoms are of course not defined by simple hard wall potentials, but the LCD and PLD still give simple interpretations for the behavior of real systems.[3] If an adsorbed molecule is larger than the PLD of a porous material, a large energetic barrier to diffusion will exist at the bottlenecks that define the PLD. Conversely, molecules significantly smaller than the PLD are able to diffuse freely through the material. The LCD indicates whether two molecules of different species will have enough space to easily pass one another inside the porous material, a factor that can be important in selecting materials for separation applications.[11]

We recently introduced efficient methods to unambiguously calculate the PLD and LCD of crystalline porous materials.[3] Briefly, a unit cell of the porous material is divided into a finely-spaced grid. After assigning a chemically-relevant hard sphere size to each atom in the porous material, the maximum diameter of a hard sphere that can be inserted at each grid point without overlapping the framework is calculated. The maximum value observed among these diameters is the LCD. The PLD is computed by using algorithms originally developed in studies of the percolation theory[12] in which sets of connected grid points are identified that all allow adsorption of a hard sphere of a chosen diameter without overlaps with the porous material. These calculations do not require any assumptions about the direction of the pores within the porous material, unlike some earlier approaches.[10] It is important to note that this approach assumes that the porous framework is rigid. We note that related ideas have been used for some time in the description of penetrant diffusion through polymers.[13]

In the next section, we discuss the PLD and LCD for a very large set of hypothetical set of silica zeolites generated by Deem *et al.*[6] In that work, candidate silica crystal structures were energetically refined using the Sanders–Leslie–Catlow (SLC) interatomic potential.[14] Crystal structures with energies less than 30 kJ mol^{-1} higher than quartz were retained. This effort generated 313 568 distinct crystal structures. 44 053 of the structures generated were found to have an energy lower than quartz, and Deem *et al.* suggested that these materials are likely to be artifacts of the force field used in the calculations. We computed the PLD and LCD of all 313 568 structures, but only the 269 515 materials with energies calculated to be higher than quartz are shown below.

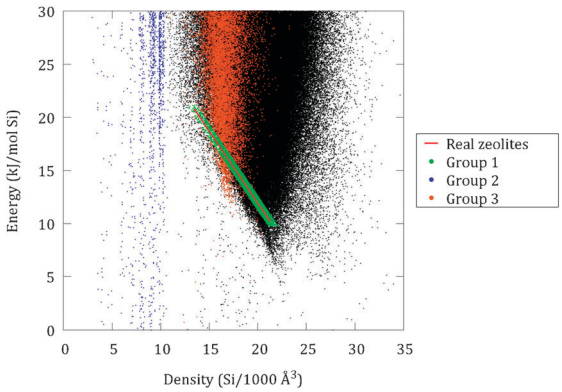

Fig. 1 Number density of Si atoms as a function of the energy per Si atom relative to quartz for 269 515 hypothetical zeolites.

In Fig. 1, the energy as calculated by Deem *et al.* for the zeolites with energies within 30 kJ mol^{-1} of quartz is shown as a function of the Si atom density. This figure has been recreated from the work by Deem *et al.*[6] The red line indicates the region where real zeolites (*i.e.* zeolites that have been observed experimentally) fall on this figure, as described by Deem *et al.*[6] Three subgroups of materials are highlighted in Fig. 1 using blue, green, and orange dots. The structures shown as green dots, denoted as Group 1, have been selected as they form the area around the location of the real zeolites and may be expected to more closely represent the variety of pore morphologies that are experimentally accessible. Although the location of these materials in Fig. 1 is similar to the real zeolites, the set of structures in Group 1 contains more materials with relatively high density than the collection of real zeolites (see Fig. 2 and 3). The structures shown as blue dots, denoted as Group 2, were selected for further analysis based on their low density values that sets them apart from the rest of the structures. The structures shown with orange dots, denoted as Group 3, have been highlighted because they form a group of structures with a large difference between their largest cavity diameter and pore limiting diameter. Groups 1 and 2 are particularly interesting because structures in Group 1 are structurally similar with zeolites that are already accessible experimentally and structures in Group 2 might be accessible

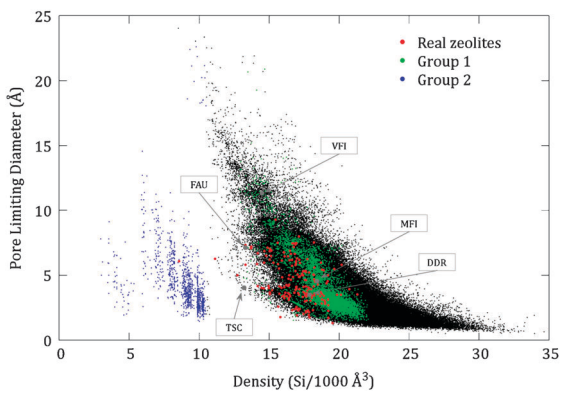

Fig. 2 The pore limiting diameter (PLD) for the complete set of materials shown in Fig. 1, with materials from Group 1, Group 2, and the real zeolites highlighted in color. Five examples of well known real zeolites are labeled.

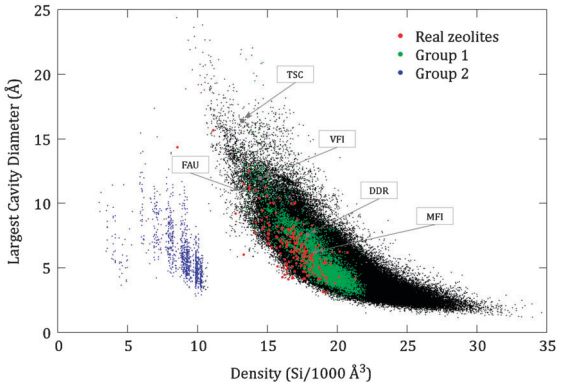

Fig. 3 The number density plotted against the LCD values for all the materials, Group 1, Group 2 and for the real zeolites.

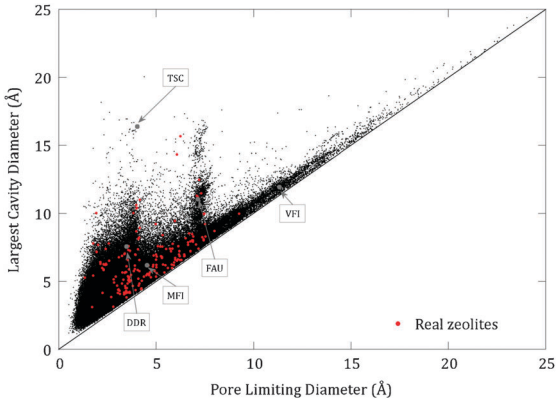

Fig. 4 The PLD printed against the LCD for all the materials and for the real zeolites.

via a crystallization pathway from a low-density solution.[6] Groups 1, 2 and 3 contain 6367, 1192, and 1829 structures, respectively.

Results—pore sizes

We used the algorithms outlined above to compute the pore limiting diameter (PLD) and largest cavity diameter (LCD) for all of the hypothetical and real materials shown in Fig. 1. The PLD for the full set of materials is shown as a function of the material density in Fig. 2. A wide range of PLDs is found, from materials that are essentially nonporous because they have PLDs < 3 Å to crystals that have very open pores with PLDs > 20 Å. The 191 real zeolites (in their ideal, silica form) are shown with red circles. Five of these zeolites are highlighted in the figure and are useful for interpreting the physical implications of the PLD. DDR is a well known zeolite with 8 membered rings (8MR), and the small size of these 8MRs allows for size discrimination between diffusing CH_4 and CO_2 molecules.[2] The somewhat larger channels in zeolite MFI allow light gases such as CH_4 and CO_2 to diffuse freely, but show size discrimination among the isomers of xylene and between linear and branched alkanes.[15–17] FAU has pores that are larger than MFI, and VFI is well known among all zeolites because of its large pore size. The pores that control molecular diffusion in VFI are 18MRs.[18]

Fig. 3 shows the largest cavity diameter (LCD) for the full set of hypothetical zeolites and the 191 real zeolites as a function of their density. As with the PLDs, a large range of LCD values are observed. The five real zeolites highlighted in this figure help illustrate the difference between the LCD and PLD. For example, the LCD of DDR is larger than for MFI, although the reverse is true for the PLD. This is a simple consequence of the observation that DDR is a cage-like zeolite whose cavities can be described as cages of moderate size connected by a small window[2] while MFI is a channel-like zeolite whose cavities are best described as a series of connected channels that are approximately cylindrical.[19] The known zeolite with the largest LCD is the TSC structure. This material has not been synthesized in a pure silica form, and was identified as the mineral tschörtnerite from natural mineral samples.[20] This material has large cages of diameter >15 Å connected by small windows defined by 8MRs.

In general, both the PLD and LCD increase with decreasing density. This is not surprising, since a low density material is expected to have larger pores than a high density material. It is interesting to note, however, that at lower densities the range of pore size values increases. For example, for a density of 15 (25) Si/1000 Å^3, the PLD varies from 2.5–20 Å (1.5–5 Å). This illustrates how two materials with the same empty space can have very different pore topologies and that small openings along the pore direction are possible even for low density materials. This variation with respect to density is less pronounced for the LCD values in Fig. 3 since the LCD is more indicative of the free volume in each structure. In both figures, the very low density materials in Group 2 have ranges of LCD and PLD values that are similar to the other more dense materials. In Fig. 4, the PLDs for the complete set of hypothetical materials are shown as a function of the LCD for the same materials. This figure also highlights the real zeolites. The black solid line in this figure indicates the limit of a perfectly cylindrical pore for which the LCD and PLD are equal. This representation of the data highlights materials such as TSC that have large cages connected by small windows. In the case of the TSC structure, the PLD is 4.02 Å and the LCD is 16.39 Å. There is a noticeable peak in the set of hypothetical materials with PLD ≈ 7 Å. We examine these materials below by defining a subset of the materials denoted Group 3. Four real zeolites fall within this area including FAU (PLD = 7.13 Å, LCD = 11.06 Å).

The data from Fig. 4 are replotted in Fig. 5 by using (LCD–PLD), a quantity that measures the size difference between the largest open volumes in a crystal and the windows that control molecular diffusion. By definition, (LCD–PLD) is a positive quantity. Several subsets of the hypothetical zeolites, denoted Groups 1, 2, and 3, are shown in Fig. 5 by plotting the negative of (LCD–PLD); this is simply done to allow the data to be clearly distinguished from the other data in the figure. Fig. 5 shows how we defined Group 3 to select materials from the pronounced peak in the (LCD–PLD) that exists for PLD ≈ 7 Å. The hypothetical materials from Groups 1 and 2, the sets with densities similar to real zeolites and with very low densities, respectively, have distributions of PLD and (LCD–PLD) that are relatively similar to the distributions for the full set of hypothetical materials. The very large

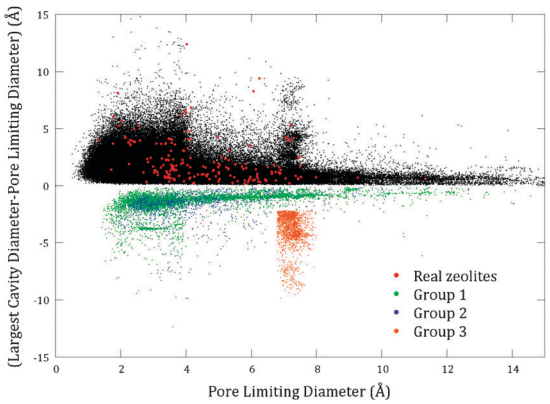

Fig. 5 (LCD–PLD) plotted as a function of PLD for the complete set of hypothetical materials and real zeolites (positive values) and for Groups 1, 2 and 3 (negative values). (LCD–PLD) is a positive quantity for all materials, but the negative of this quantity is shown for Groups 1, 2, and 3 for visual clarity. 269 hypothetical materials with PLD > 15 Å are not shown.

number of hypothetical zeolites examined in our calculations makes it difficult to determine from the figures discussed up to this point the fraction of structures that have pore characteristics of a particular type. One way to examine this point is to calculate the normalized frequency of observing materials with a particular set of pore characteristics among the full set of materials, as is shown in Fig. 6. In this figure, the frequency scale was defined by counting the number of structures in bins of area 0.05 × 0.05 Å and normalizing the largest value to 1. This examination shows that the majority of the crystal structures (~57% of the complete set of structures) have PLDs between 1.7 and 4 Å and (LCD–PLD) between 0.5 and 2.5 Å. This implies that a large fraction of the hypothetical zeolites are essentially nonporous; any material with a PLD significantly less than 4 Å will not allow diffusion of any but the smallest gas molecules.

Another view of the distribution of pore sizes is given in Fig. 7 and 8 where the PLD and (LCD–PLD) are shown in the form of histograms for the hypothetical and real zeolites. For each set of materials, the histogram is normalized to give a total area of 1. One interesting observation from these histograms is that they are quite smooth for the hypothetical

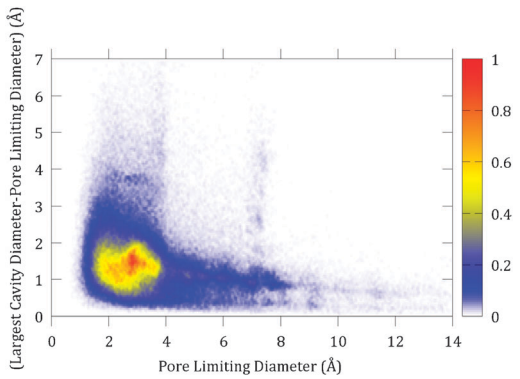

Fig. 6 The frequency of observing crystal structures with varying PLD and (LCD–PLD) among the full set of hypothetical zeolites. The normalization used for the color code is defined in the text.

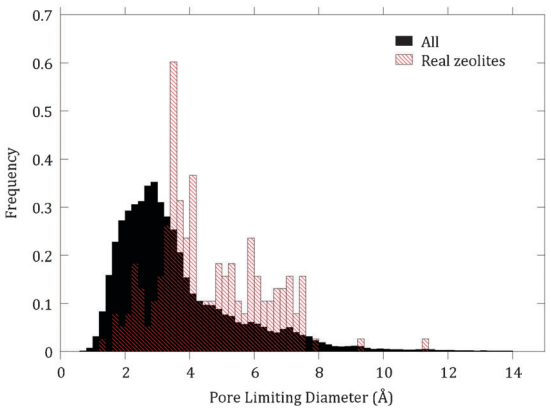

Fig. 7 Histogram showing the normalized frequency of structures as a function of PLD for the hypothetical and real zeolites. The frequency has been normalized so that both histograms give an area of 1.

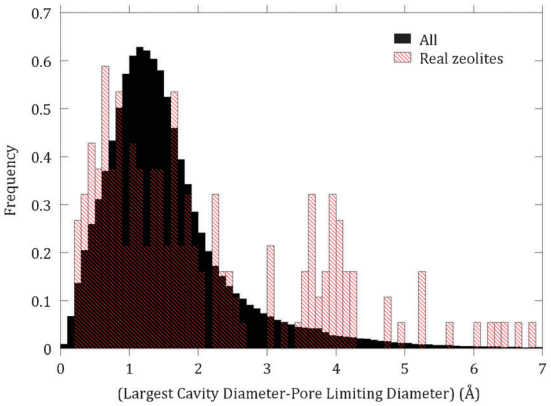

Fig. 8 Histogram showing the normalized frequency of structures as a function of (LCD–PLD) for the hypothetical and real zeolites. The frequency has been normalized so that both histograms give an area of 1.

zeolites, even though zeolite pore openings are defined by rings with discrete numbers of atoms (8MRs, 10MRs, *etc.*). The absence of pronounced peaks in the PLD histogram occurs because distortions in the shape of these rings, and minor differences in the atomic positions making up the rings, allow a large variety of pore widths to exist. This observation could reasonably be deduced from the variety of real zeolites that are known, but as the data in Fig. 7 show it would be relatively difficult to test this idea in a quantitative way from the limited data available with real materials. This discussion illustrates the unsurprising observation that it is important to know the actual geometry of a pore opening, not simply the ring size, in order to understand how a zeolite might show size discrimination among molecules with similar sizes. It is also clear from Fig. 7 and 8 that the histograms for real zeolites and the hypothetical zeolites define rather different distributions, with the hypothetical zeolites being strongly weighted towards materials with low porosity. It is very likely that this simply reflects the nature of synthesis methods for zeolites, which prominently feature structure directing agents that almost by definition (if successful) yield porous materials.

The analogous histograms for the materials in Groups 1 and 2 are compared with the full set of hypothetical zeolites in

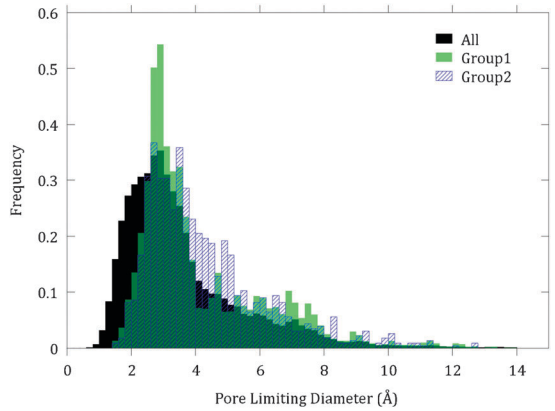

Fig. 9 Histogram showing the normalized frequency of structures as a function of PLD for the complete set of hypothetical zeolites and Groups 1 and 2. The frequency has been normalized so that both histograms give an area of 1.

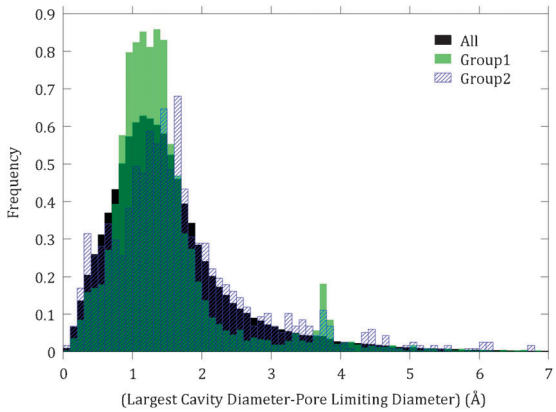

Fig. 10 Histogram showing the normalized frequency of structures as a function of (LCD-PLD) for the complete set of hypothetical zeolites and Groups 1 and 2. The frequency has been normalized so that both histograms give an area of 1.

Fig. 9 and 10. These groups do not contain the highest density materials found among the hypothetical structures, so their PLDs tend to be somewhat larger on average than the full set of materials. In both groups, however, a significant fraction of the materials have PLD < 4 Å.

Results—energetics

In order to better characterize the performance of nanoporous materials for use in molecular separations, interactions between the framework and the adsorbed species need to be defined by introducing an interatomic potential. In our earlier work, we showed that it is possible to efficiently compute Henry's constants for adsorption and the energy barrier to diffusion for a large set of porous materials by extending the methods used above once an interatomic potential is chosen.[3] These two quantities give valuable information about the selectivity of a material for adsorption-based separations or kinetic-based separations. While they cannot give a full description of each material because they neglect effects from adsorbate–adsorbate interactions, they can still be used to rapidly identify and eliminate large numbers of materials that

Table 1 Lennard-Jones values for CH_4[21]–zeolite and H_2[22]–zeolite interactions

	ε/k_B/K	σ/Å
Ozeo-CH_4	133	3.214
Ozeo-H_2	72	2.708

are irrelevant for a given separation, thereby saving a great deal of experimental effort.

The way that we calculated the Henry's constant and diffusion activation energy was described in detail in our earlier work.[3] Briefly, the Henry's constant is calculated *via* a weighted integral of the energy of an adsorbed molecule over the volume of one unit cell of the material.[23,24] The diffusion activation energy is calculated by examining the grid points that make up the major pore. The first step is to identify the largest energy value of a grid point that is required in order to form a complete path across the pore of the structure. This corresponds to the energy value at the bottleneck of the pore. The energy barrier is then estimated as the difference between the energy at the bottleneck and lowest energy value found in the structure. By assuming that diffusion is governed by the hopping rate over this single energetic barrier an estimate for diffusion can be given. These calculations require the same assumptions of the geometric analysis in the previous section, namely the porous material is assumed to be rigid and the method is applicable to spherical adsorbates. The interactions between CH_4 or H_2 and each zeolite were defined by a pairwise sum of Lennard-Jones potentials for the interaction energy between an adsorbed molecule and O atoms in the zeolite, with numerical parameters taken from previous modeling studies. The parameters of these interaction potentials are given in Table 1. We examined the hypothetical zeolites in Group 1 and Group 2, as well as the full set of experimentally observed zeolites (in their all-silica form) using these methods for CH_4 and H_2 at 298 K. Below we show data only for CH_4; the analogous data for H_2 are given in the ESI.†

Fig. 11 shows the Henry's constant for CH_4 at room temperature plotted against the largest cavity diameter for the structures in Group 1 and Group 2 as well as the real zeolites. The trends in Henry's constants for H_2 (Fig. S5 in the ESI†) are similar. The observed results can be separated into

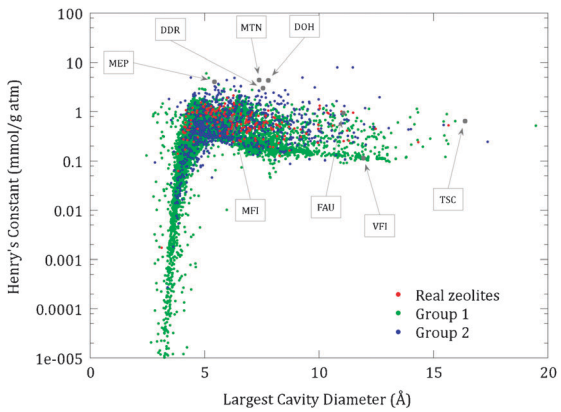

Fig. 11 Henry's constant for CH_4 plotted against the LCD values for the structures in Group 1, Group 2 and the real zeolites.

two parts. The first part corresponds to the case where the cavity is too small to accommodate a CH_4 molecule without strong overlap with the framework atoms. This results in very small values for the Henry's constant, which become smaller as the largest pore diameter value decreases. The second behavior seen in these results corresponds to the situation where one or more cavities are large enough to accommodate CH_4 without overlap. If adsorption takes place only in the cavity that corresponds to the largest cavity diameter then as the cavity size increases a maximum is observed when CH_4 can access a position in the center of the cavity and maximize its interaction with the surrounding framework atoms. As the cavity size increases beyond this point, a CH_4 molecule can only maximize its interactions with a fraction of the framework atoms that make up the cavity, leading to a decrease in the overall Henry's constant. This maximum appears in Fig. 11 for materials with LCD $\approx$ 5 Å, although a considerable amount of scatter exists around this value. Some structures in Group 2 have large values of Henry's constant when the LCD is considerably larger than 5 Å. This occurs because of the existence of secondary cavities in the structure that offer very highly favorable interactions to CH_4. We note that in these calculations we considered all the cavities present in the unit cell to be accessible to CH_4. If a more detailed study was performed, it would be important to exclude any non-accessible volume.

A number of real zeolites are highlighted in Fig. 11, where we have chosen these materials to span a range of pore diameters. The range of Henry's constants for CH_4 among the highlighted materials is quite similar to the overall range spanned by the hypothetical zeolites we examined.

The calculated energy barrier for diffusion in CH_4 for the zeolites in Groups 1 and 2 and the real zeolites are shown in Fig. 12. Similar data for diffusion of H_2 are shown in Fig. S6 in the ESI.† In this case, the results are plotted as a function of the pore limiting diameter. When the PLD is smaller than the size of the adsorbate, the overlap with the framework atoms at the bottleneck of the pore leads to a very high energy barrier to diffusion and an exponential dependence on the PLD. In these cases, the most important part of the interactions of the adsorbate with the framework is the repulsive interactions with the framework atoms at the bottleneck. For larger values of the PLD, the net energy barrier depends on the relative strength of the interactions both at the adsorption site and the bottleneck of the pore. In this regime, the calculated energy barrier to diffusion is small (typically <10 kJ mol^{-1}), and there is considerable scatter in the energy barriers observed among materials with similar PLDs.

When the net energy barrier to diffusion is large relative to thermal energies, transition state theory (TST) gives reliable estimates for the net hopping rate between energy minima. A simple formulation of TST that can be applied to a large number of materials is to estimate the self-diffusivity of an adsorbate as[2,3,25] $D_s = ka^2/2$, where k is the hopping rate over the rate-controlling barrier and a is the characteristic distance for a hop. We estimated the hopping rate using $k = \nu\exp(-\Delta E/k_BT)$, where the pre-exponential factor ν was assumed to be 10^{11}. We calculated the single-component diffusivity for CH_4 at 303 K using this TST description for 10 real zeolite frameworks (Table 2). The distance used as the hopping distance was defined manually from the experimental structure for each case by taking twice the cavity to bottleneck distance. In several cases (VFI, CAN, CFI, MTW, MER, ETR, MAZ and LTF) it was found that the hopping distance is equal to the smallest crystallographic axis, while for the zeolite with structure code DFT it is half that value. The distances used are listed in the ESI† in Table S1. It should also be noted that if the distance used is taken as half of the average value of the three crystallographic axes the results do not differ considerably for most cases we examined. This more approximate approach has the advantage that the distance can be determined automatically.

The diffusion coefficients predicted by this simplified version of TST are compared to observations from Molecular Dynamics (MD) simulations for these 10 materials in Table 2. In order for the results to be directly comparable to the TST calculations, the MD simulations were performed under infinite dilution conditions; in other words no adsorbate–adsorbate interactions were considered. Each simulation run was equilibrated with 1.5×10^7 Grand Canonical Monte Carlo (GCMC) moves and 1.5×10^7 MD steps. Data were collected from MD runs which were 20 ns in duration using 1 fs time-steps and 30 independent trajectories were used to calculate the self-diffusivity. Other details of the

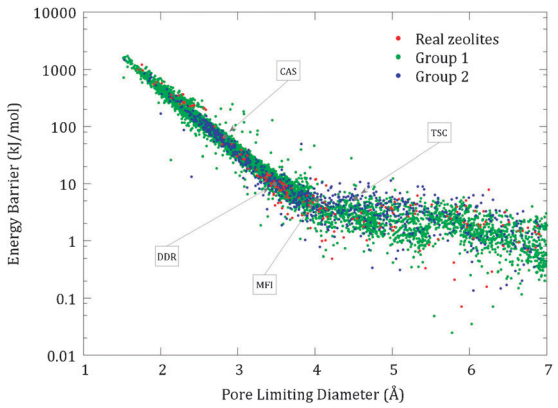

Fig. 12 The energy barrier to diffusion of CH_4 plotted against the PLD values for the structures in Group 1, Group 2 and the real zeolites.

Table 2 Single component diffusivities for CH_4 at 303 K for 10 zeolites as computed from Molecular Dynamics and the simplified TST approach described in the text. The calculated energy barrier for each material is also shown, as is the ratio of the two calculated diffusivity values for each material. The materials are listed in the ascending order for the energy barrier and the units are cm^2 s^{-1} for the diffusivity and kJ mol^{-1} for the energy barrier

	D_s from MD	D_s from TST	ΔE	D_s^{MD}/D_s^{TST}
VFI	2.8×10^{-4}	3.66×10^{-4}	0.02	0.78
CAN	6.56×10^{-4}	1.34×10^{-4}	0.07	4.89
CFI	4.54×10^{-4}	1.33×10^{-4}	0.11	3.42
MTW	5.37×10^{-4}	9.07×10^{-5}	1.06	5.92
TSC	3.9×10^{-5}	1.51×10^{-4}	5.18	0.26
MER	2.47×10^{-5}	1.2×10^{-5}	9.31	2.01
DDR	1.40×10^{-6}	6.32×10^{-6}	9.89	0.22
DFT	4.73×10^{-6}	1.82×10^{-6}	10.13	2.59
GOO	8.24×10^{-9}	4.79×10^{-9}	26.98	1.72
CAS	$<10^{-8}$	4.77×10^{-16}	66.39	N/A

MD simulations were chosen from previous work by Jee and Sholl.[2] It should be noted that using MD simulations with a duration of $\sim$10 ns is only capable of measuring diffusivities as low as 10^{-8} cm^2 s^{-1}, since slower diffusion than this value gives net mean squared displacements of <1 Å within the simulation time. This is the case for the zeolite CAS and therefore we do not list a diffusivity value calculated from MD for this material in Table 2.

The agreement between our MD simulations and the simple TST estimates is quite good. The materials we examined were chosen so that they span a range of energy barrier values, in part to determine whether a systematic deviation from the TST results exists for smaller barriers. Somewhat surprisingly, no such trend was observed and our TST calculations were able to yield semi-quantitative predictions for every material for which MD was also applicable. The TST approach is of course also useful for materials such as CAS where MD is not applicable because of the slow diffusion of the adsorbate. A useful conclusion from this comparison is that a screening procedure based on the energy barriers calculated from our geometric analysis can successfully rank materials based on the diffusivity values for a given spherical adsorbate.

It is important to note that the calculated diffusion coefficient for adsorbates in materials with relatively small PLDs can be sensitive to the choice of the force field used to define adsorbate–framework interactions. To give a specific example, Jee and Sholl showed that the kind of generic force field we have used in the calculations reported above significantly overestimates the diffusivity of CH_4 in DDR when compared with experimental observations.[2] This led to the development of an improved force field that described both the adsorption and diffusion of CH_4 in this 8MR zeolite more accurately. This example, and the examples given above, where TST and/or MD can be used to understand molecular diffusion in detail, illustrate the methods that are available to examine specific zeolites once materials have been chosen from the large number of possible materials that exist. The value of the approximate estimates available from Fig. 12 and the simplified TST approach we have discussed is that these estimates quickly classify large number of materials in terms of their diffusion properties. This efficient classification creates opportunities to focus attention on the most promising materials for applications where diffusion is critical and motivates more detailed studies of these materials.

To illustrate one such approach to screening materials for possible applications, we show in Fig. 13 Henry's constants for CH_4 at room temperature plotted against the energy barrier to diffusion for the materials in Group 1, Group 2, and the real zeolites. The structures in the upper part of the figure could be considered for kinetic separations in which the objective is to exclude CH_4 because of the large diffusion activation energies (*i.e.* very slow diffusion) of CH_4 in these materials. The bottom right part of the figure includes structures with significant affinity towards CH_4 but also low enough energy barrier values that the diffusion of CH_4 in these materials is not prohibitively slow. These materials could potentially be useful in adsorption-based separations where the objective is to adsorb significant amounts of CH_4. It is interesting to note in Fig. 13 that for Group 1, the predicted Henry's constant is

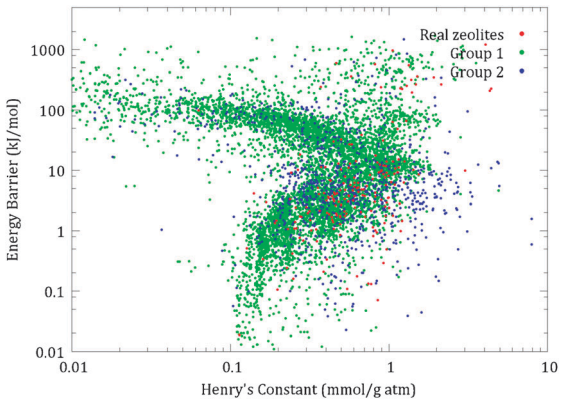

Fig. 13 The energy barrier to diffusion of CH_4 plotted against the Henry's constant for CH_4 for the structures in Group 1, Group 2 and the real zeolites.

negatively correlated with the predicted diffusion activation energy for materials with activation energies larger than $\sim$10 kJ mol^{-1}, but positively correlated for materials with lower activation energies. There is little evidence for a similar correlation, however, among the materials in Group 2 or the real zeolites.

Conclusion

We have used efficient computational methods to characterize the pore sizes of $>250\,000$ hypothetical silica zeolites. These calculations provide information on the largest cavities that are available to adsorbing molecules in each zeolite and information on the range of adsorbate molecules that can feasibly diffuse through each zeolite. We have compared the properties of the hypothetical zeolites we examined with the complete set of experimentally known zeolite crystal structures. These properties are computed in a purely geometric manner. For a subset of $\sim$8000 zeolites, we performed a more detailed analysis that predicted the Henry's constant and diffusion activation energy for two prototypical small molecule adsorbates, CH_4 and H_2. Once the diffusion activation energy is available from these calculations, a simple version of transition state theory (TST) can be used to estimate the diffusivity of each adsorbate. We performed MD simulations for a limited number of zeolites chosen to show a range of diffusion activation energies, and found that our simple TST estimates for self-diffusion were in semi-quantitative agreement with the MD results, even for materials with very low energy barriers to diffusion. Taken together, our calculations demonstrate a useful set of methods for rapidly assessing the properties of adsorbates in very large collections of zeolites and other nanoporous crystalline materials.

We conclude by commenting on several limitations of our current approach and the relation between our methods and other well known modeling methods for nanoporous crystals. In this paper, we only examined pure silica materials. We have shown in earlier work on MOFs, however, that our methods are well suited to describing libraries of crystalline materials made from a diverse range of chemical building blocks.[3] Our methods are currently limited to spherical adsorbates, although extending them to rigid molecules where orientational

effects would be important is not difficult to imagine. Analyzing the diffusion of the largest spherical constituent of a molecule that is nonspherical would be one simple way to make useful estimates of whether these molecules can or cannot readily diffuse through a crystalline material of interest that requires no effort beyond what we have already demonstrated in this paper.

Our methods are also limited to adsorbates at infinite dilution. We do not view this as a strong limitation to the usefulness of the methods. A host of well-developed molecular simulation methods exist that allow the adsorption and diffusion of adsorbates as pure components and as adsorbed mixtures at an arbitrary density in a microporous material. Once a material is found to have some interesting properties for dilute adsorbate loadings using our efficient methods, these more detailed methods can readily be used to generate accurate information at any adsorbate concentration of interest. This idea illustrates the more general point that the methods described here are best used as one step in an integrated series of modeling tools that can rapidly examine very large numbers of candidate materials with efficient but approximate methods and then focus attention on a small number of especially promising materials where more detailed (but more time consuming) methods can be applied.

Acknowledgements

This work was supported by the ConocoPhillips Company.

Notes and references

1 S. M. Auerbach, K. A. Carrado and P. K. Dutta, *Handbook of Zeolite Science and Technology*, CRC Press, 2003.
2 S. E. Jee and D. S. Sholl, *J. Am. Chem. Soc.*, 2009, **131**, 7896–7904.
3 E. Haldoupis, S. Nair and D. S. Sholl, *J. Am. Chem. Soc.*, 2010, **132**, 7528–7539.
4 D. S. Sholl, *Acc. Chem. Res.*, 2006, **39**, 403–411.
5 F. J. Keil, R. Krishna and M. O. Coppens, *Rev. Chem. Eng.*, 2000, **16**, 71–197.
6 M. W. Deem, R. Pophale, P. A. Cheeseman and D. J. Earl, *J. Phys. Chem. C*, 2009, **113**, 21353–21360.
7 M. M. J. Treacy, I. Rivin, E. Balkovsky, K. H. Randall and M. D. Foster, *Microporous Mesoporous Mater.*, 2004, **74**, 121–132.
8 M. D. Foster, A. Simperler, R. G. Bell, O. D. Friedrichs, F. A. A. Paz and J. Klinowski, *Nat. Mater.*, 2004, **3**, 234–238.
9 Ch. Baerlocher and L. B. McCusker, Database of Zeolite Structures: http://www.iza-structure.org/databases/.
10 M. D. Foster, I. Rivin, M. M. J. Treacy and O. Delgado Friedrichs, *Microporous Mesoporous Mater.*, 2006, **90**, 32–38.
11 T. Watanabe, S. Keskin, S. Nair and D. S. Sholl, *Phys. Chem. Chem. Phys.*, 2009, **11**, 11389–11394.
12 J. Hoshen and R. Kopelman, *Phys. Rev. B*, 1976, **14**, 3438–3438.
13 M. L. Greenfield and D. N. Theodorou, *Macromolecules*, 1993, **26**, 5461–5472.
14 M. J. Sanders, M. Leslie and C. R. A. Catlow, *J. Chem. Soc., Chem. Commun.*, 1984, 1271.
15 K. Beschmann, G. T. Kokotailo and L. Riekert, *Chem. Eng. Process.*, 1987, **22**, 223–229.
16 S. Namba, *Zeolites*, 1984, **4**, 77–80.
17 G. Xomeritakis, Z. Lai and M. Tsapatsis, *Ind. Eng. Chem. Res.*, 2001, **40**, 544–552.
18 M. E. Davis, C. Saldarriaga, C. Montes, J. Garces and C. Crowdert, *Nature*, 1988, **331**, 698–699.
19 G. T. Kokotailo, S. L. Lawton, D. H. Olson and W. M. Meier, *Nature*, 1978, **272**, 437–438.
20 H. Effenberger, G. Giester, W. Krause and H. J. Bernhardt, *Am. Mineral.*, 1998, **83**, 607.
21 A. I. Skoulidas and D. S. Sholl, *J. Phys. Chem. B*, 2002, **106**, 5058–5067.
22 E. D. Akten, R. Siriwardane and D. S. Sholl, *Energy Fuels*, 2003, **17**, 977–983.
23 R. L. June, A. T. Bell and D. N. Theodorou, *J. Phys. Chem.*, 1990, **94**, 1508–1516.
24 K. Watanabe, *J. Chem. Soc., Faraday Trans.*, 1991, **87**, 1951–1958.
25 D. M. Ford and E. D. Glandt, *J. Phys. Chem.*, 1995, **99**, 11543–11549.

